STAT2 deficiency and susceptibility to viral illness in humans

Sophie Hambleton[a,b,1], Stephen Goodbourn[c], Dan F. Young[d], Paul Dickinson[e], Siti M. B. Mohamad[a,f], Manoj Valappil[g], Naomi McGovern[a], Andrew J. Cant[a,b], Scott J. Hackett[h], Peter Ghazal[e], Neil V. Morgan[i], and Richard E. Randall[d,1]

[a]Primary Immunodeficiency Group, Institute of Cellular Medicine, Newcastle University, Newcastle upon Tyne NE2 4HH, United Kingdom; [b]Pediatric Immunology Service, Great North Children's Hospital, Newcastle upon Tyne NE1 4LP, United Kingdom; [c]Division of Biomedical Sciences, St. George's, University of London, London SW17 0RE, United Kingdom; [d]School of Biology, University of St. Andrews, Fife KY16 9TS, United Kingdom; [e]Division of Pathway Medicine, University of Edinburgh, Edinburgh, EH16 4SB, United Kingdom; [f]Advanced Medical and Dental Institute, Universiti Sains Malaysia, 11800 USM Penang, Malaysia; [g]Health Protection Agency, Royal Victoria Infirmary, Newcastle upon Tyne NE1 4LP, United Kingdom; [h]Pediatric Immunology Department, Heartlands Hospital, Birmingham B9 5SS, United Kingdom; and [i]Centre for Cardiovascular Sciences, Institute for Biomedical Research, University of Birmingham, Birmingham B15 2TT, United Kingdom

Edited* by Robert A. Lamb, Northwestern University, Evanston, IL, and approved January 10, 2013 (received for review November 22, 2012)

Severe infectious disease in children may be a manifestation of primary immunodeficiency. These genetic disorders represent important experiments of nature with the capacity to elucidate nonredundant mechanisms of human immunity. We hypothesized that a primary defect of innate antiviral immunity was responsible for unusually severe viral illness in two siblings; the proband developed disseminated vaccine strain measles following routine immunization, whereas an infant brother died after a 2-d febrile illness from an unknown viral infection. Patient fibroblasts were indeed abnormally permissive for viral replication in vitro, associated with profound failure of type I IFN signaling and absence of STAT2 protein. Sequencing of genomic DNA and RNA revealed a homozygous mutation in intron 4 of *STAT2* that prevented correct splicing in patient cells. Subsequently, other family members were identified with the same genetic lesion. Despite documented infection by known viral pathogens, some of which have been more severe than normal, surviving STAT2-deficient individuals have remained generally healthy, with no obvious defects in their adaptive immunity or developmental abnormalities. These findings imply that type I IFN signaling [through interferon-stimulated gene factor 3 (ISGF3)] is surprisingly not essential for host defense against the majority of common childhood viral infections.

measles vaccine | viruses | rare diseases

Innate immune responses play a key role in controlling microbial infections by interfering with the replication and/or viability of the invading microbe, and favoring the development of adaptive immunity. Foremost among innate antiviral defenses is the IFN response. IFNs are a group of cytokines secreted as a direct consequence of pathogen exposure, by most cell types (innate IFN, types I and III) or by activated T and NK lymphocytes, in the context of an overall immune response (type II, i.e., IFN-γ). The importance of IFN is emphasized by the fact that most viruses have evolved strategies to evade this response (1). Indeed, viruses generally lose pathogenicity when their defined IFN antagonists are knocked out. Furthermore, marked susceptibility to viral infection has been observed in mice with genetic lesions of the IFN signaling pathway [e.g., *Ifnar1* (2), *Stat1* (3, 4) or *Stat2* (5)].

IFNs mediate their biological activity by up-regulating the expression of hundreds of diverse IFN-stimulated genes (ISGs), the products of which may have direct or indirect antiviral activity. Most cell types can respond to type I IFN (as IFN-β and multiple IFN-α subclasses) as well as IFN-γ, whereas there is more limited tissue distribution of the receptor for type III IFN (IFN-λ1, -λ2, and -λ3). Binding of IFN-α/β to the type I IFN receptor (IFNAR) causes activation of the receptor-associated kinases Jak1 and Tyk2, which in turn phosphorylate and activate the signal transduction and activators of transcription STAT1 and STAT2. These associate with IRF9 to form the heterotrimeric transcription factor, ISGF3, that binds to IFN-stimulated response elements (ISREs) to activate the promoter of IFN-α/β–stimulated genes (6). Although type III IFNs bind to a distinct receptor, this agonizes the same signaling pathway as IFNAR, and hence produces a similar transcriptional profile (7). In contrast, ligation of the IFN-γ receptor activates Jak1 and Jak2 to phosphorylate STAT1 (but not STAT2), which homodimerizes to form the GAF transcription factor that binds to GAS elements in the regulatory regions of IFN-γ–induced genes. It should also be noted that IFN-α/β also weakly activates GAF as a result of STAT1 phosphorylation; furthermore, certain ISGs can be induced by IRFs, themselves activated by viral infection directly (8, 9) or following IFN induction.

Primary immunodeficiency disorders (PIDs) provide an opportunity to scrutinize the importance of individual genes and pathways in human immunity, yet isolated susceptibility to viral infections has rarely been recognized as a PID phenotype (10, 11). Autosomal-recessive STAT1 deficiency in humans produces a severe primary immunodeficiency characterized by susceptibility to lethal viral and mycobacterial disease (12,13). In this context, we now report the surprisingly mild phenotype of human STAT2 deficiency. Despite a profoundly defective innate IFN response, and evident susceptibility to some viral infections, STAT2-deficient individuals can cope well with the majority of common viruses and lead a relatively healthy life.

Results

We evaluated a 5-y-old child with a history of disseminated vaccine-strain measles, a highly unusual complication despite widespread vaccine use (14). Six days after routine vaccination aged 18 mo, the patient developed fever, rash, conjunctivitis, and lymphadenopathy, followed by hepatitis and pneumonitis requiring supplemental oxygen. Vaccine-strain measles was detected by PCR in bronchoalveolar lavage and in blood as late as 14 d after vaccination. This child recovered with supportive care, but an infant sibling later died suddenly in the context of a 2-d febrile illness, with features of overwhelming viral infection postmortem.

Author contributions: S.H., S.G., P.G., N.V.M., and R.E.R. designed research; S.H., S.G., D.F.Y., P.D., S.M.B.M., M.V., N.M., A.J.C., S.J.H., N.V.M., and R.E.R. performed research; S.H., S.G., P.D., P.G., N.V.M., and R.E.R. analyzed data; and S.H. and R.E.R. wrote the paper.

The authors declare no conflict of interest.

*This Direct Submission article had a prearranged editor.

Freely available online through the PNAS open access option.

Data deposition: The data reported in this paper have been deposited in dbSNP (accession no. ss706293995) and the Gene Expression Omnibus (GEO) database, www.ncbi.nlm.nih.gov/geo (accession no. GSE41960).

[1]To whom correspondence may be addressed. E-mail: sophie.hambleton@ncl.ac.uk or rer@st-andrews.ac.uk.

This article contains supporting information online at www.pnas.org/lookup/suppl/doi:10.1073/pnas.1220098110/-/DCSupplemental.

The presence of parental consanguinity further raised suspicion of an autosomal recessive PID. However, no predisposition to bacterial infection in the proband was evident, and growth and development were normal.

As neither history nor laboratory evaluation suggested a T- or B-cell immunodeficiency (Table S1), we pursued the hypothesis that a novel defect of innate immunity had produced this apparently selective susceptibility to viral infection. As an initial screen, we compared the ability of primary skin fibroblasts from the index patient and a healthy control subject to support viral plaque formation in vitro (Fig. 1*A*). Strikingly, all the WT viruses tested formed significantly larger plaques on the patient's cells than the control cells, including influenza A virus and parainfluenza viruses. Furthermore, the attenuated vaccine strain of measles could produce plaques on patient cells, in contrast to control cells (Fig. 1*A*). These in vitro findings indeed suggested an innate susceptibility to viral infection in the proband.

To explore this further, we used highly attenuated recombinant strains of PIV5 (PIV5VΔC) and Bunyamwera virus (BUNΔNSs) that lack defined functional IFN antagonists (15, 16). These viruses form pinpoint plaques (PIV5VΔC) or cannot form plaques (BUNΔNSs) in cells that produce and respond to IFN (Fig. 1*B*), but grow readily if the IFN system is disabled, for instance, by engineering cells to express the V protein of PIV5 that targets STAT1 for proteasome-mediated degradation (17, 18) (Fig. 1*B*; see Fig. 4*A* for STAT1 deficiency and IFN-α–unresponsiveness of V protein-expressing cells). Strikingly, patient cells supported the formation of large plaques of PIV5VΔC and BUNΔNSs (Fig. 1*B*), implying a complete failure of the type I IFN response.

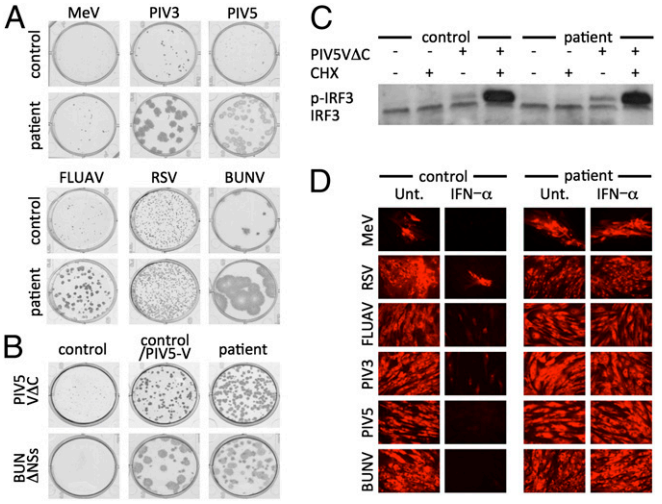

Fig. 1. Patient dermal fibroblasts have a major defect in their IFN system. (*A*) Relative plaque sizes of a panel of negative-strand RNA viruses [vaccine strain measles virus (MeV), parainfluenza virus types 3 and 5 (PIV3, PIV5), influenza A virus (FLUAV), respiratory syncytial virus (RSV), and Bunyamwera virus (BUNV)] in patient and control cells. Monolayers of cells were virally infected, and fixed at 4 d postinfection (p.i.); plaques were visualized by immunostaining. (*B*) Relative plaque sizes of IFN-sensitive viruses PIV5VΔC and BUNΔNSs in control cells, those rendered IFN-unresponsive by forced expression of PIV5-V (control/PIV5-V, see text), or patient cells. (*C*) Activation (phosphorylation) of IRF3 in patient and control cells. Fibroblast monolayers were or were not infected with the vM2 preparation of PIV5VΔC (19) in the presence or absence of cycloheximide (CHX; 50 μg/mL). At 10 h p.i., cell lysates were made and the presence of p-IRF3 detected by immunoblot analysis. Note that more p-IRF3 is detected in the presence of CHX than in its absence because activated IRF3 induces a ubiquitin ligase that targets p-IRF3 for proteasome-mediated degradation (9). (*D*) Monolayers of control and patient cells were, or were not (Unt.), pretreated with IFN-α for 15 h before infection with a panel of negative-sense RNA viruses at a multiplicity of infection of 0.2 to 10 pfu/cell. At 48 h p.i., virus-infected cells were visualized by immunofluorescence.

To investigate the mechanism of this susceptibility, we first tested whether patient fibroblasts could produce IFN in response to virus infection (19). No impairment was observed in the phosphorylation of IRF3 (Fig. 1*C*) or the subsequent production of IFN (Fig. S1). We therefore compared the ability of patient and control cells to develop an antiviral state in response to exogenous IFN-α, challenging them with the same panel of viruses tested in the plaque assays, and visualizing viral replication by immunofluorescence (Fig. 1*D*). These results demonstrated a remarkable lack of protection in the patient's cells, establishing a severe defect in their ability to respond to IFN-α.

To dissect this impaired IFN response, we used immunoblotting to monitor the induction of selected ISGs in patient and control fibroblasts that were treated with IFN-α or IFN-γ, or infected by virus (Fig. 2*A*). As expected, STAT1 was phosphorylated and later induced by IFN-α and IFN-γ in the control cells, and a similar result was seen in the patient's cells (Fig. 2*A* and Fig. S2), demonstrating intact GAF signaling downstream of both IFN receptors. Although MxA and ISG56/IFIT1 were up-regulated by IFN-α in the control cells, they were completely refractory to induction in the patient cells, suggesting a block in signaling via ISGF3. ISG56/IFIT1 could be induced upon infection of patient cells with virus, consistent with the observation that IRF3 activation was intact (Fig. 1*C*) and that IRF3 itself can up-regulate ISG56 expression but not that of MxA (8, 9, 20). Neither gene was up-regulated by IFN-γ.

To obtain a more global view of the response to IFN, we undertook whole-genome transcriptional profiling of fibroblasts treated for 10 h in the presence or absence of IFN-α. In keeping with the previously noted pattern, the IFN response of patient cells was largely ablated in terms of the number of transcripts up-regulated (~10% of control; Fig. 2 *B* and *C*). Among the 284 genes that were up-regulated at least twofold in control cells but not in patient cells, were many classical targets normally strongly induced by IFN, e.g., Mx1, Mx2, OAS1, OAS2, and OAS3 (167-, 49-, 68-, 40-, and 30-fold induction in control cells, respectively). The residual transcriptional response in patient cells, which largely overlapped that of control (Fig. 2*C*), was blunted for every gene except IRF1, suggesting partial activation (Fig. S3). We therefore examined the promoter elements of the differentially expressed genes for the presence of ISRE, GAS, and IRF1 binding sites by using the oPOSSUM database (21) (Fig. 2*D*). The few ISRE-containing genes that were up-regulated by IFN-α in patient cells also contained GAS elements and/or IRF1 sites, and could thus have been up-regulated independently of ISGF3.

Given these results, we next examined the integrity of individual ISGF3 components in patient fibroblasts (Fig. 3*A*). Whereas IRF9 and STAT1 were readily detected, there was no detectable expression of STAT2 as determined by immunoblotting with antibodies against the C terminus (Fig. 3*A*) or N terminus (Fig. S4). The complete lack of STAT2 provided a ready explanation for the failure to induce ISGs dependent upon activation by the ISGF3 complex. Genomic patient DNA was therefore subjected to sequencing of the *STAT2* gene, disclosing WT sequence except for a single variant within the donor splice site of introns 4 and 5 (c.381+5 G>C; Fig. 3*B*) that was absent from databases of genetic variation (Ensembl release 67; National Center for Biotechnology Information) and from 218 ethnically matched control chromosomes sequenced. Both affected siblings were homozygous for this variant whereas the parents and a healthy sibling (V5) were heterozygous (Fig. 3*C*).

G at position c.381+5 is highly conserved among *STAT2* orthologues from armadillo to mouse and apes, and its substitution by C was predicted to destroy the donor splice site of intron 4 by three alternative splicing prediction programs [Netgene2 (22), human splicing finder 2.4.1 (23), and NNSPLICE 0.9 (24)]. We therefore

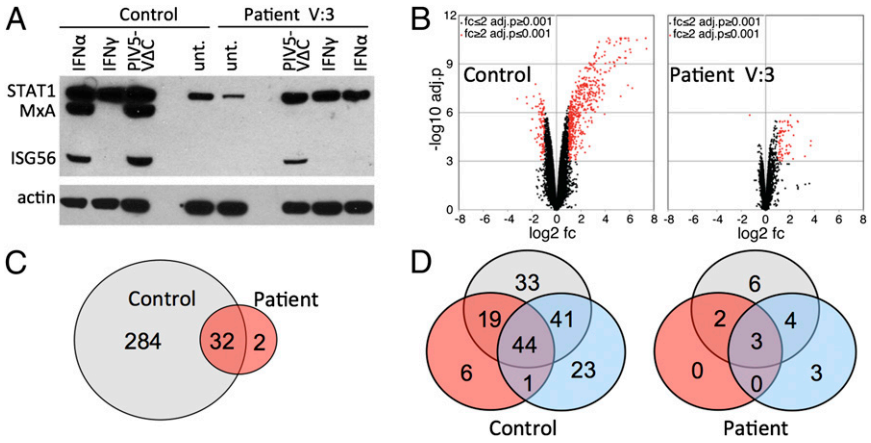

Fig. 2. Patient cells fail to up-regulate ISGF3-dependent genes in response to IFN-α. (*A*) Control and patient skin fibroblasts were treated for 18 h with IFN-α or IFN-γ, infected with the vM2 preparation of PIV5VΔC for 18 h, or left untreated (Unt.). Total cell lysates were immunoblotted for STAT1, MxA, IFIT1/ISG56, and actin. (*B–D*) Whole genome microarray analysis of the transcriptional response to IFN-α in control and patient cells. (*B*) Volcano plots show the effect of IFN-α treatment of control and patient fibroblasts for 10 h. Data are plotted for all 29,298 probes used ($\log_2$ fold change on the *x* axis, $-\log_{10}$-adjusted *P* value on the *y* axis) to show significance of expression change after treatment. Probes with at least twofold change (positively or negatively regulated) and adjusted $P \leq 0.001$ are shown in red; those not significantly changed (i.e., less than twofold) are in black. (*C*) Venn diagram shows genes up-regulated in control and patient cells following IFN-α treatment. Numbers of genes showing at least twofold change and adjusted $P \leq 0.001$ cutoff are shown. Genes in control cells are shown in gray, genes in patient cells are shown in red. (*D*) Venn diagrams to show numbers of differentially expressed genes with predicted binding sites for the indicated transcription factors within 10,000 bp of their promoter. ISRE-containing genes are shown in red, IRF1 consensus binding site-containing genes are shown in gray, and GAS-containing genes are shown in blue.

investigated the effect of the mutation on splicing of *STAT2* mRNA by reverse transcriptase (RT)-PCR analysis of cDNA derived from the index patient, family and control cells. To look in detail at the splicing of intron 4, we performed a PCR with primers anchored in exons 3 and 6, separated the reaction products by gel electrophoresis and sequenced individual bands (Fig. 3 *D* and *E*). Whereas control cells produced a single band, corresponding to fully spliced mRNA, two longer PCR products were obtained from V.3, neither of which was correctly spliced. The larger product retained intron 4 in its entirety, whereas a minor product (similar in size to WT band) had been cryptically spliced and retained 17 nt from intron 4. Heterozygous relatives generated a mixture of all three bands, as expected.

In further analysis, we amplified full length *STAT2* mRNA from V.3 and control by using primers anchored in the untranslated leader and trailer sequences. The patient product was revealed to be longer and less abundant than control, consistent with aberrant splicing and presumably nonsense-mediated decay (Fig. S5). Sequencing revealed that the major full-length transcript in the patient retained intron 4 and intron 6 and lacked exons 16 and 17

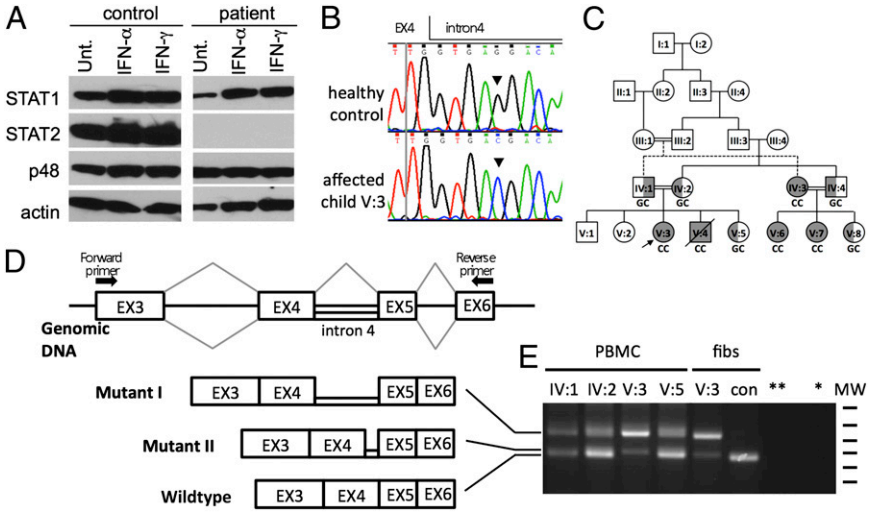

Fig. 3. Loss of ISGF3 activity reflects the absence of STAT2, caused by a homozygous splicing mutation in intron 4 of *STAT2*. (*A*) Total cell lysates of patient and control cells that had, or had not (Unt.), been treated with IFN-α or IFN-γ for 18 h were immunoblotted for STAT1, STAT2, IRF9, and actin. (*B*) Capillary sequencing traces from healthy control (*Upper*) and affected child V.3 (*Lower*) demonstrate homozygous G>C variant at position c.381+5. (*C*) Pedigree from a consanguineous family (roman numerals refer to the generation, numbers the individuals) with susceptibility to severe viral illness. Letters beneath family member represent the genotype [i.e., homozygous (CC; filled boxes) or heterozygous (GC; half-filled boxes) for the G>C variant at position c.381+5; unfilled boxes indicate unknown zygosity]. Proband is indicated by an arrow, line through V:4 indicates deceased. (*D*) Schematic showing exon structure of genomic DNA of *STAT2* between exons 3 and 6. (*E*) Agarose gel electrophoresis of products obtained from RT-PCR by using primers anchored in exons 3 and 6 of *STAT2* (indicated in *D*) and template cDNA from the indicated family members or control, together with schematic showing mutant and natively spliced mRNA species.

as a result of splicing of exon 15 to a cryptic acceptor in intron 17, thus incorporating extra material 5′ to exon 18. This implies unexpectedly long-range effects of the c.381+5 G>C mutation on mRNA splicing. Readthrough into intron 4 would be predicted to result in a highly truncated protein, but, by immunoblotting with an antibody directed against the N terminus, we were unable to demonstrate any such fragment of STAT2 in patient cells (Fig. S4).

In the extended family, (pedigree is detailed Fig. 3*C*, in which each member is coded with a roman numeral to designate their generation and a number), we subsequently discovered three further homozygotes for the c.381+5 G>C variant, including a 6-y-old child (V.6) with a history of a prolonged febrile encephalitic illness days after measles/mumps/rubella (MMR) vaccination. Both she and V.7 (who had not been immunized for MMR) had been hospitalized for viral illness on one other occasion, but the recent infection history of their homozygous mother IV.3 was unremarkable (childhood history was not available). We confirmed that homozygosity for the c.381+5 G>C mutation correlated with the lack of STAT2 protein and an inability to up-regulate MxA in response to IFN-α in leukocytes [i.e., peripheral blood mononuclear cells (PBMCs)] obtained from the proband (V3) and her aunt (IV:3), in contrast to the control and heterozygous family members (IV:2, IV:4, and V5; Fig. S6). Thus, STAT2 could not be detected, and MxA was not up-regulated by IFN, in skin fibroblasts or in PBMCs homozygous for the c.381+5 G>C variant, consistent with a pervasive defect in IFN signaling.

The conjunction of undetectable STAT2 expression, together with profound unresponsiveness to IFN-α [as well as the inability of PIV5 to target STAT1 for proteasome-mediated degradation in the patient's cells, a process that is absolutely dependent on the presence of STAT2 (25); Fig. S7], implied that patient cells were effectively STAT2-null. To establish beyond doubt that deficiency of STAT2 was responsible for the in vitro susceptibility phenotype, we transduced the patient fibroblasts with a lentiviral vector encoding WT STAT2 and documented the restoration of type I IFN responsiveness, as indicated by both up-regulation of antiviral ISGs (Fig. 4*A*) and resulting protection against viral infection (Fig. 4 *B* and *C*).

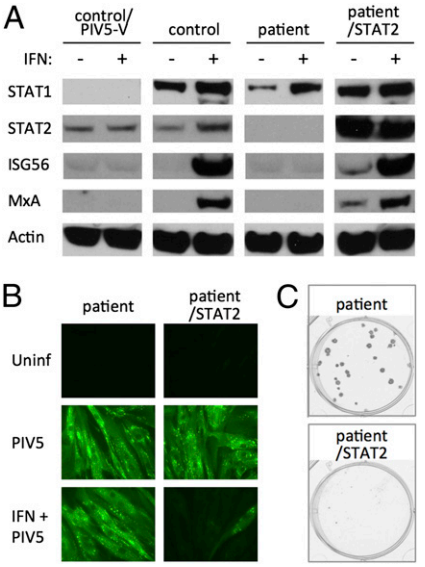

Fig. 4. Lentiviral transduction of STAT2 into patient cells restores their ability to respond to IFN-α and induce an antiviral state. (*A*) Control and V:3 patient skin fibroblasts, patient cells that had been genetically engineered to express STAT2 (patient/STAT2), and control cells that expressed the V protein of PIV5 (control/PIV5-V) that targets STAT1 for proteasome-mediated degradation (Fig. S7) were treated for 18 h with IFN-α or left untreated. Total cell lysates were immunoblotted for STAT1, STAT2, ISG56, MxA, and actin. (*B*) Monolayers of patient and patient/STAT2 cells were, or were not, pretreated with IFN-α for 15 h before mock infection (Uninf) or infection with PIV5 at 10 pfu/cell. At 24 h p.i., virus-infected cells were visualized by immunofluorescence. (*C*) Relative plaque size of PIV5VΔC in unmodified patient cells and patient cells expressing STAT2. Monolayers of cells were infected with PIV5VΔC, and fixed at 4 d p.i.; plaques were visualized by immunostaining.

Discussion

STAT2 c.381+5 G>C represents a splicing mutation, and our virally susceptible patients exhibited this previously unreported PID, STAT2 deficiency. Mutations within *Stat2* in mice have been linked to viral susceptibility in vivo and in vitro, considered to reflect the nonredundant role of this molecule in signaling by type I and type III IFNs. Stat2-null mice were reported to be almost as vulnerable to vesicular stomatitis virus infection as Stat1-null mice (5). In contrast, we find the viral-susceptibility phenotype of human STAT2 deficiency to be considerably milder than has been described for children with autosomal-recessive STAT1 deficiency (12, 13). The five cases of STAT2 deficiency we report within this single kindred range in clinical phenotype from asymptomatic (healthy adult) to fatal (death in infancy from overwhelming viral illness). All three surviving affected children have had hospital admissions for viral illness, and both of those who received MMR vaccine became ill with definite (V.3) or probable (V.6) dissemination of vaccine-strain virus. However, other viral illnesses have generally been mild (Table S2 lists documented infection history and limited serology); for example, three of the five have experienced unremarkable varicella (the other surviving child remains varicella zoster virus-naive). Furthermore the proband (V:3) experienced primary HSV infection as gingivostomatitis, whereas one of the STAT1-deficient individuals described by Dupuis et al. died of HSV encephalitis (12), and severe susceptibility to herpesviral disease appears general in complete STAT1 deficiency (13). HSV encephalitis susceptibility in humans has also been linked to mutations that specifically impair viral IFN induction (26–29). The fact that herpesvirus disease severity appears relatively normal in STAT2 deficiency implies that loss of ISGF3-dependent signaling is unlikely to represent the sole mechanism for herpesviral susceptibility in these disorders.

The particular patterns of susceptibility seen in these rare PIDs must reflect the altered balance between host defenses and the virulence and immune evasion strategies of those pathogens encountered (30). In this light, the evident virulence of vaccine strain measles toward STAT2-deficient individuals confirms that IFN sensitivity is critical to the attenuation of this virus, which displays wider tissue tropism than its parent (31). On the host side, the variable and age-dependent expressivity of the STAT2-deficient phenotype recalls the behavior of innate immune disorders affecting TLR signaling pathways (26, 29, 32, 33). Although children with the latter disorders are at high risk of invasive bacterial infection, those who survive beyond childhood outgrow this susceptibility, perhaps as a result of the development of adaptive immunity.

Our clinical and biochemical data suggest that GAF-dependent signaling is functionally intact in STAT2 deficiency, not only within the IL-12/IFN-γ pathway but also downstream of the IFNAR. This finding is at odds with a previous report suggesting that STAT2 is required to recruit STAT1 to the IFNAR, based on impairment of STAT1 phosphorylation in a STAT2-deficient cell line (34). In Stat2-KO mice, however, Park et al. noted that this effect was tissue-specific and reflected variable reduction in basal Stat1 expression (5). Similarly, we also noted reduced basal STAT1 expression in our STAT2-deficient patient fibroblasts (Figs. 2*A* and 3*A*) that was corrected by STAT2 transduction (Fig. 4*A*). This may reflect the operation of a STAT2-dependent autocrine loop whereby constitutively expressed type I IFN contributes to

maintenance of STAT1 expression (reviewed in ref. 35). Nonetheless, our data show robust IFN-α–dependent phosphorylation of STAT1 in patient cells (Fig. S2), suggesting that its recruitment to the IFN-α/β receptor is independent of STAT2. Naturally we cannot completely rule out the possibility that there is a small amount of a N-terminally truncated form of STAT2—which we failed to detect—that can perform this function.

Type I IFN exerts important effects within the adaptive immune system, where it has been reported to modulate T-cell and antigen-presenting cell behavior (36). However, the extent to which this is STAT2-dependent is unclear, especially because alternative IFN signaling pathways operate within different leukocyte subsets (6, 37). Reduced splenic dendritic cell numbers were noted in a Stat2-hypomorphic mouse strain (38), but we found normal abundance of myeloid and plasmacytoid dendritic cell as well as monocytes in peripheral blood of the index patient (Fig. S8). Remarkably, the proband showed evidence of normal adaptive immunity in positive antibody titers against live vaccines (i.e., MMR), killed vaccines (i.e., tetanus, *Haemophilus influenzae* type b, pneumococcus), and naturally encountered pathogens (i.e., influenza H1N1, adenovirus, and EBV; Table S2); she also exhibited full suppression of EBV in peripheral blood. Hence, we conclude that ISGF3-mediated IFN signaling is dispensable for adaptive immunity *in natura*. Furthermore, even though ISGF3-dependent induction of ISGs with direct antiviral activity (such as MxA) clearly aids resistance to viral infections, it is by no means essential for host defense against common viral pathogens in humans. This is extremely surprising given the critical role of IFN in the induction of an antiviral state in uninfected cells, thereby slowing the spread of virus from the initial focus of infection. Although many ISGs may be activated by other transcription factors [including IRF1 (39)], such ISGF3-independent activation usually occurs only within virally infected cells. Thus, recognition of this unusual PID phenotype challenges understanding of the concerted antiviral immune response and provides an important model in which to define the role of innate IFN and its interaction with viral pathogenesis in humans.

Materials and Methods

Cells. The study was performed with approval from the National Research Ethics Service. Clinical samples were obtained with informed consent according to the Declaration of Helsinki. PBMCs and primary dermal fibroblast cultures were obtained by standard methods. The latter were cultured in DMEM with 10% (vol/vol) FCS and supplemental penicillin and streptomycin. To generate control cells expressing the V protein of PIV5 and patient cells expressing functional STAT2, the PIV5 V gene and the full-length ORF of STAT2 were cloned into the bicistronic lentivirus vector (pHR-SIN-CSGW); lentiviruses were produced and the cells were transduced and selected for puromycin resistance as described previously (40). The full-length ORF of human STAT2 was amplified by using specific primers by reverse transcription (Superscript III; Invitrogen) and PCR (HiFi DNA polymerase; Kappa Biosystems), using total RNA from control patient fibroblast cells. The insert was initially cloned into pJET1.2 and sequenced, and then the insert was transferred into the lentivirus vector.

Viruses and Interferons. The viruses used have been described previously (41), apart from measles virus, which was the Enders attenuated Edmonston strain. IFN-α [Roferon A (Roche) or Intron A (Schering-Plough)] and IFN-γ (R & D Systems; or Immukin (Boehringer)] were used at 1,000 IU/mL.

Plaque assays were performed by standard methods in six-well dishes that included 0.1% Avicel (FMC Biopolymer) or 1% agarose (influenza A virus only; Biogene) in the overlay medium. Plaques were visualized by immunostaining by using a pool of monoclonal antibodies or polyclonal antisera specific for the different viruses as described previously (41), together with alkaline phosphatase-conjugated secondary antibody by using SIGMAFAST BCIP/NBT as the substrate.

Immunoblotting and immunofluorescence procedures for fibroblasts have previously been described (19). Virus-specific antibodies have been described by Chen et al. (41). Antibodies specific for MxA, ISG56 (IFIT1), STAT1, C-terminal STAT2, IRF3, and IRF9 were purchased from Santa Cruz (cat. nos. sc50509, sc82946, sc417, sc476, sc9082, and sc496, respectively), pSTAT1 from Upstate (nos. 07-302 and 07-307), p-IRF3 from Cell Signaling Technology (no. 4947), β-actin from Sigma (no. A 5441), and GAPDH from Abcam (no. ab8245). Immunofluorescence was examined with a Nikon Microphot-FXA immunofluorescence microscope.

PBMCs were seeded in a 24-well plate at 2×10^6 cells per well in 1 mL of RPMI medium with 10% FCS, incubated at 37 °C in 5% CO_2, and stimulated with IFN-α overnight as described earlier. After harvesting by centrifugation, cells were lysed in 20 mM Tris HCl, pH 7.4, 150 mM NaCl, 1% Triton X-100, 5 mM EDTA, 100 mM DTT (Sigma-Aldrich), and NUPAGE LDS Sample Buffer (Invitrogen). Lysates were subjected to electrophoresis and immunoblotting as described earlier.

Mutation Screening. The 23 coding exons and exon–intron boundaries of *STAT2* were PCR-amplified with specific intronic primers designed using exon-primer (http://ihg.gsf.de/ihg/ExonPrimer.html; primer sequences are available on request). Sequencing was performed using standard methods on an ABI 3730 automated sequencer (Applied Biosystems). Genomic DNA from 218 ethnically matched controls was used to screen for the identified *STAT2* mutation.

RT-PCR. Total RNA was isolated from fibroblasts by using Tri-Reagent (Sigma) and used as a template for oligo-dT–primed reverse transcription using SuperScript III (Invitrogen; Fig. S5). Aliquots of the RT reaction were used in PCR amplifications with HiFi DNA polymerase (Kapa Biosystems) and the following primers: for full-length ORF, STAT2 forward (5′-CCCCCATGGCGCAGTGGGAAATGCTG-3′) plus STAT2 reverse (5′-GGGGAATTCCTAGAAGTCAGAAGGCATC-3′); N-terminal fragment, STAT2 forward plus STAT2 SacLow (5′-CAATGGGAGCTCTGATGCAGG-3′).

Alternatively, for exons 3 to 6, total RNA was extracted from human PBMCs or fibroblasts by using the RNeasy Mini Kit (Qiagen). cDNA was synthesized by using random primers and AMV reverse transcriptase by using Promega reverse transcription system A3500 according to the manufacturer's instructions. RT-PCR of exons 3 to 6 was performed by using the following primers: STAT2_cDNAF (5′-CCAAGGCTACCATGCTATTC-3′) and STAT2_cDNAR (5′-GCTGGTCTTTCAGTTGGCTG-3′).

Microarray Analysis. Patient (V:3) and control fibroblasts were cultured in DMEM containing 10% FCS in 24-well plates and treated with 1,000 U/mL IFN-α for 10 h or given a mock treatment ($n = 4$). Cells were lysed with QIAgen RLT plus buffer and RNA was isolated by using the QIAgen RNeasy Plus kit. RNA concentration and purity were obtained by spectrophotometry, and RNA integrity was monitored using a model 2100 Bioanalyzer system (Agilent). Fifty nanograms of total RNA were used to synthesize biotinylated cRNA target, which was hybridized to the Human PrimeView GeneChip (Affymetrix) according to the manufacturer's instructions. Data from hybridized chips were acquired by using proprietary Affymetrix platform scanners and AGCC software (Affymetrix). The numeric data were processed and subsequently analyzed with the Bioconductor package (42) for the R statistical programming environment. Raw data distributions and summary statistics were assessed for quality. Data were then background-corrected, quantile-normalized, and probe-set–summarized by using the RMA algorithm (43). A nonspecific expression-level filter was applied to remove probes that were not expressed on any of the samples in the experiment, and the remaining 29,298 probes were used for statistical analysis. Null hypotheses for each probe were based on the comparison between mock and IFN-α–treated samples; they were tested by using an empirical Bayes test, providing good robustness for small sample sizes (44). To adjust for multiple testing issues, the false discovery rate was controlled by using the Benjamini–Hochberg *P* value adjustment method (45). Probes were interpreted on the basis of the fold change of differential expression between mock and IFN-α treatment and the corresponding statistical significance. Microarray data have been deposited in the Gene Expression Omnibus database with accession code GSE41960. Differentially expressed genes were analyzed for overrepresented conserved transcription factor binding sites in the promoter sequence (±10,000 bases) by single site analysis by using oPOSSUM database 3.0 (21) with a conservation cutoff of 0.4 and matrix score threshold of 85%. Promoters were examined for the presence of ISGF3 (ISRE), IRF1, and STAT1 (GAS) binding sites.

Serologic Assessment of Adaptive Immunity. Serum antibody responses to influenza A(H1N1) pdm09, A(H3N3), and influenza B viruses were detected by hemagglutination inhibition assay (HI) by using previously described methods (46). Samples with titers ≥32 by HI were considered positive. Antibody responses to other natural and vaccine antigens were assessed by routine diagnostic methods (adenovirus by complement fixation, other antigens by commercial ELISAs; details available on request).

ACKNOWLEDGMENTS. We thank the subjects' families for their trust, our many colleagues in National Health Service hospitals and laboratories who contributed to patient care, and Catherine Thompson and colleagues at the Respiratory Virus Unit, Health Protection Agency (London, United Kingdom), where influenza serology was assessed. This work was supported by Medical Research Council Fellowship G0701897 (to S.H.), the Bubble Foundation (S.H.), and Wellcome Trust Grants AL087751/B (to S.G.) and 087751/A/08/Z (to R.E.R.).

1. Randall RE, Goodbourn S (2008) Interferons and viruses: An interplay between induction, signalling, antiviral responses and virus countermeasures. *J Gen Virol* 89(pt 1):1–47.
2. Müller U, et al. (1994) Functional role of type I and type II interferons in antiviral defense. *Science* 264(5167):1918–1921.
3. Durbin JE, Hackenmiller R, Simon MC, Levy DE (1996) Targeted disruption of the mouse Stat1 gene results in compromised innate immunity to viral disease. *Cell* 84(3): 443–450.
4. Meraz MA, et al. (1996) Targeted disruption of the Stat1 gene in mice reveals unexpected physiologic specificity in the JAK-STAT signaling pathway. *Cell* 84(3): 431–442.
5. Park C, Li S, Cha E, Schindler C (2000) Immune response in Stat2 knockout mice. *Immunity* 13(6):795–804.
6. Platanias LC (2005) Mechanisms of type-I- and type-II-interferon-mediated signalling. *Nat Rev Immunol* 5(5):375–386.
7. Zhou Z, et al. (2007) Type III interferon (IFN) induces a type I IFN-like response in a restricted subset of cells through signaling pathways involving both the Jak-STAT pathway and the mitogen-activated protein kinases. *J Virol* 81(14):7749–7758.
8. Fensterl V, Sen GC (2011) The ISG56/IFIT1 gene family. *J Interferon Cytokine Res* 31(1): 71–78.
9. Killip MJ, Young DF, Precious BL, Goodbourn S, Randall RE (2012) Activation of the beta interferon promoter by paramyxoviruses in the absence of virus protein synthesis. *J Gen Virol* 93(pt 2):299–307.
10. Dropulic LK, Cohen JI (2011) Severe viral infections and primary immunodeficiencies. *Clin Infect Dis* 53(9):897–909.
11. Zhang SY, et al. (2008) Inborn errors of interferon (IFN)-mediated immunity in humans: Insights into the respective roles of IFN-alpha/beta, IFN-gamma, and IFN-lambda in host defense. *Immunol Rev* 226:29–40.
12. Dupuis S, et al. (2003) Impaired response to interferon-alpha/beta and lethal viral disease in human STAT1 deficiency. *Nat Genet* 33(3):388–391.
13. Boisson-Dupuis S, et al. (2012) Inborn errors of human STAT1: Allelic heterogeneity governs the diversity of immunological and infectious phenotypes. *Curr Opin Immunol* 24(4):364–378.
14. Demicheli V, Rivetti A, Debalini MG, Di Pietrantonj C (2012) Vaccines for measles, mumps and rubella in children. *Cochrane Database Syst Rev* 2:CD004407.
15. He B, et al. (2002) Recovery of paramyxovirus simian virus 5 with a V protein lacking the conserved cysteine-rich domain: the multifunctional V protein blocks both interferon-beta induction and interferon signaling. *Virology* 303(1):15–32.
16. Weber F, et al. (2002) Bunyamwera bunyavirus nonstructural protein NSs counteracts the induction of alpha/beta interferon. *J Virol* 76(16):7949–7955.
17. Didcock L, Young DF, Goodbourn S, Randall RE (1999) The V protein of simian virus 5 inhibits interferon signalling by targeting STAT1 for proteasome-mediated degradation. *J Virol* 73(12):9928–9933.
18. Young DF, et al. (2003) Virus replication in engineered human cells that do not respond to interferons. *J Virol* 77(3):2174–2181.
19. Killip MJ, et al. (2011) Failure to activate the IFN-β promoter by a paramyxovirus lacking an interferon antagonist. *Virology* 415(1):39–46.
20. Holzinger D, et al. (2007) Induction of MxA gene expression by influenza A virus requires type I or type III interferon signaling. *J Virol* 81(14):7776–7785.
21. Ho Sui SJ, et al. (2005) oPOSSUM: Identification of over-represented transcription factor binding sites in co-expressed genes. *Nucleic Acids Res* 33(10):3154–3164.
22. Brunak S, Engelbrecht J, Knudsen S (1991) Prediction of human mRNA donor and acceptor sites from the DNA sequence. *J Mol Biol* 220(1):49–65.
23. Desmet FO, et al. (2009) Human Splicing Finder: An online bioinformatics tool to predict splicing signals. *Nucleic Acids Res* 37(9):e67.
24. Reese MG, Eeckman FH, Kulp D, Haussler D (1997) Improved splice site detection in Genie. *J Comput Biol* 4(3):311–323.
25. Parisien JP, Lau JF, Rodriguez JJ, Ulane CM, Horvath CM (2002) Selective STAT protein degradation induced by paramyxoviruses requires both STAT1 and STAT2 but is independent of alpha/beta interferon signal transduction. *J Virol* 76(9):4190–4198.
26. Casrouge A, et al. (2006) Herpes simplex virus encephalitis in human UNC-93B deficiency. *Science* 314(5797):308–312.
27. Pérez de Diego R, et al. (2010) Human TRAF3 adaptor molecule deficiency leads to impaired Toll-like receptor 3 response and susceptibility to herpes simplex encephalitis. *Immunity* 33(3):400–411.
28. Sancho-Shimizu V, et al. (2011) Herpes simplex encephalitis in children with autosomal recessive and dominant TRIF deficiency. *J Clin Invest* 121(12):4889–4902.
29. Guo Y, et al. (2011) Herpes simplex virus encephalitis in a patient with complete TLR3 deficiency: TLR3 is otherwise redundant in protective immunity. *J Exp Med* 208(10): 2083–2098.
30. Nish S, Medzhitov R (2011) Host defense pathways: role of redundancy and compensation in infectious disease phenotypes. *Immunity* 34(5):629–636.
31. Shingai M, et al. (2007) Differential type I IFN-inducing abilities of wild-type versus vaccine strains of measles virus. *J Immunol* 179(9):6123–6133.
32. Zhang SY, et al. (2007) TLR3 deficiency in patients with herpes simplex encephalitis. *Science* 317(5844):1522–1527.
33. Picard C, Casanova JL, Puel A (2011) Infectious diseases in patients with IRAK-4, MyD88, NEMO, or IκBα deficiency. *Clin Microbiol Rev* 24(3):490–497.
34. Leung S, Qureshi SA, Kerr IM, Darnell JEJ, Jr., Stark GR (1995) Role of STAT2 in the alpha interferon signaling pathway. *Mol Cell Biol* 15(3):1312–1317.
35. Gough DJ, Messina NL, Clarke CJ, Johnstone RW, Levy DE (2012) Constitutive type I interferon modulates homeostatic balance through tonic signaling. *Immunity* 36(2): 166–174.
36. Welsh RM, Bahl K, Marshall HD, Urban SL (2012) Type 1 interferons and antiviral CD8 T-cell responses. *PLoS Pathog* 8(1):e1002352.
37. van Boxel-Dezaire AH, et al. (2010) Major differences in the responses of primary human leukocyte subsets to IFN-beta. *J Immunol* 185(10):5888–5899.
38. Chen LS, et al. (2009) STAT2 hypomorphic mutant mice display impaired dendritic cell development and antiviral response. *J Biomed Sci* 16:22.
39. Schoggins JW, Rice CM (2011) Interferon-stimulated genes and their antiviral effector functions. *Curr Opin Virol* 1(6):519–525.
40. Hilton L, et al. (2006) The NPro product of bovine viral diarrhea virus inhibits DNA binding by interferon regulatory factor 3 and targets it for proteasomal degradation. *J Virol* 80(23):11723–11732.
41. Chen S, et al. (2010) Heterocellular induction of interferon by negative-sense RNA viruses. *Virology* 407(2):247–255.
42. Gentleman RC, et al. (2004) Bioconductor: Open software development for computational biology and bioinformatics. *Genome Biol* 5(10):R80.
43. Bolstad BM, Irizarry RA, Astrand M, Speed TP (2003) A comparison of normalization methods for high density oligonucleotide array data based on variance and bias. *Bioinformatics* 19(2):185–193.
44. Smyth GK (2004) Linear models and empirical bayes methods for assessing differential expression in microarray experiments. *Stat Appl Genet Mol Biol* 3:Article3.
45. Benjamini Y, Hochberg Y (1995) Controlling the false discovery rate: A practical and powerful approach to multiple testing. *J R Stat Soc, B* 57:289–300.
46. Hardelid P, et al. (2010) Assessment of baseline age-specific antibody prevalence and incidence of infection to novel influenza A/H1N1 2009. *Health Technol Assess* 14(55): 115–192.